

Article

Electrostatic Interpretation of Phase Separation Induced by Femtosecond Laser Light in Glass

Bertrand Pommellec , Maxime Cavillon  and Matthieu Lancry 

Institut de Chimie Moléculaire et des Matériaux d'Orsay, UFR Sciences, Université Paris-Saclay, CNRS, 91405 Orsay, France

* Correspondence: bertrand.pommellec@universite-paris-saclay.fr

Abstract: Numerous studies on the effect of the femtosecond laser pulses in oxide glasses have been achieved over the last two decades, and several specific effects pointed out. Some of them are classical with respect to a laser treatment, such as thermally related effects, and are widely taken into account for applications. Other effects are directly induced by light, caused by its intricate spatiotemporal structure and associated properties: ponderomotive and polarization effects or coherence within the focal volume. These effects enable the development of forces that can lead to orientation effects. Among the specific resulting transformations from the light-induced effects in glass, the formation of so-called nanogratings was first pointed out in 2003 in silica glass. From this date, asymmetric organization into parallel nanoplanes, perpendicular to the laser polarization, have been found in many vitreous and crystalline compounds. While it is accepted that they arise from the same origin, i.e., a plasma organization that is eventually imprinted inside the material, uncertainties remain on the formation process itself. Indeed, since it exists several categories of nanogratings based on the final structuring (nanoporous phase separation, crystallization, and nanocracks), it can be expected that several processes are at the roots of such spectacular organization. This paper describes an approach based on electrochemical potential modified by an electronic excitation. The electric field induced during this process is first calculated, with a maximum of ~ 4500 kV/ μm and a distribution confined within the lamella period. The maximal chemical potential variation is thus calculated, in the studied conditions, to be in the kJ/mol range, corresponding to a glass-to-crystal phase transition energy release. The kinetics aspect of species mobility is subsequently described, strengthening the proposed approach.

Keywords: femtosecond laser induced transformations; laser induced crystallization; crystallization from glass; phase separation; silicate glass



Citation: Pommellec, B.; Cavillon, M.; Lancry, M. Electrostatic

Interpretation of Phase Separation Induced by Femtosecond Laser Light in Glass. *Crystals* **2023**, *13*, 393.

<https://doi.org/10.3390/cryst13030393>

Academic Editor: Vladimir Chvykov

Received: 18 January 2023

Revised: 17 February 2023

Accepted: 19 February 2023

Published: 24 February 2023



Copyright: © 2023 by the authors. Licensee MDPI, Basel, Switzerland. This article is an open access article distributed under the terms and conditions of the Creative Commons Attribution (CC BY) license (<https://creativecommons.org/licenses/by/4.0/>).

1. Introduction

One of the most spectacular effects of the interaction of tightly focused femtosecond (fs) laser pulses inside or at the surface of materials is the production of a special nanostructure called nanogratings (NG) or “Type II” modification regime. One example, inscribed in silica (SiO_2) glass, is provided in Figure 1. Inside the focal volume (here approximately $3 \mu\text{m}$ and $25 \mu\text{m}$ in width and length, respectively), the observed contrast takes the shape of dashes or lamellae, which are parallel to each other and perpendicular to the laser polarization orientation. After the discovery of these structures inside silica glass in 2003 [1], the substructure was found to be similar to an assembly of disks being a few μm in diameter [2].

This exemplar of NGs is the conventional view, since most of the work has been carried out in silica glass. But they have also been observed and reported in many other solid compounds. Overall, NGs can be sorted into several categories. The most popular, as mentioned above, is the one primarily revealed in SiO_2 with an arrangement of porous nanoplanes containing spherical nanopores of 10–20 nm diameter in size [1]. It is

produced by oxide decomposition due to local temperature increase [3], sensitive to the laser polarization, and giving rise to form birefringence with a large retardance amplitude as a resulting property. This type of NGs induced in volume and by femtosecond (fs) laser were observed in several glasses or crystals, including doped silica with F, P, Ge, Cl, OH [4], GeO₂ glass [5–7], SiO₂-GeO₂ glasses [8,9], TiO₂-SiO₂ glasses [10,11], TeO₂ single crystal [12], sapphire [13], Al₂O₃-Dy₂O₃ binary glass [14], lithium niobium silicate [15], or titanium silicate glasses (ULE, Corning) [11] and even in multicomponent aluminoborosilicate glasses (Borofloat 33, Schott) [11]. In β -Ga₂O₃ [16,17] and in the Ba₂O₃-GeO₂-Ga₂O₃ glass family (BGG) doped with Na, K, or La, there is no laser irradiation conditions pointing out NG formation, although doping with Ta, Gd, or Zn showed otherwise [18,19]. This is an example to highlight that a small addition of dopants can significantly impact the dynamics of NGs formation.

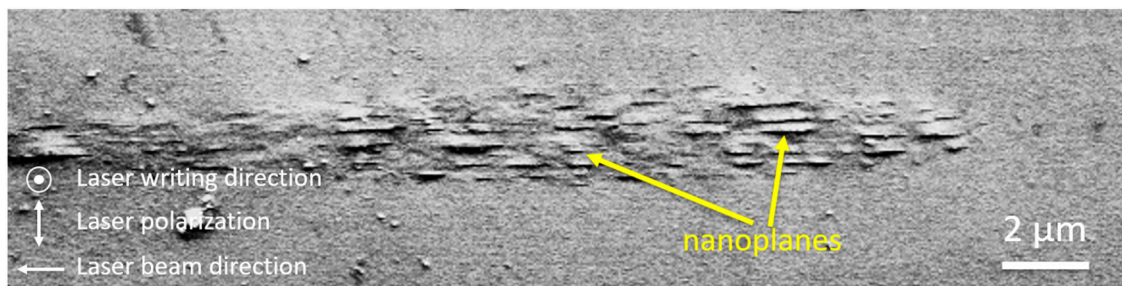


Figure 1. Structure of nanograting in pure SiO₂, observed by scanning electron microscopy (SEM) analysis of the cross section after writing a line with the following parameters: wavelength = 800 nm, pulse energy = 0.4 μ J/pulse, pulse duration = 160 fs, repetition rate = 200 kHz, numerical aperture (NA) = 0.5, and writing speed = 100 μ m/s.

To continue the above list, NGs were obtained in aluminosilicate families [19–21], i.e., aluminosilicate glasses including B₂O₃, Na₂O, and/or CaO that can vary in a large proportion. NGs are also found in crystals with small forbidden gaps such as Si, GaP, 4H-SiC, GaN, or GaS [22]. In recent work, the possibility to inscribe NGs was shown in sodium borosilicate glass (SBS) with the molar composition of 68% SiO₂, 27% B₂O₃, 4% Na₂O, and 1% Al₂O₃ [23]. This composition lies in the range of metastable liquation, which makes it possible to form a phase-separated structure in it by means of thermal treatment. Microregions with polarization-sensitive birefringence are formed when typ. $\geq 10^5$ fs laser pulses are deposited inside the glass. The laser pulse energy range enabling the formation of nanogratings and the phase shift obtained in the birefringent regions increase with the increasing number of writing pulses, and the formation of nanogratings is accompanied by the migration of sodium cations outside the laser-modified region.

Additionally, nanogratings inscription was demonstrated in nanoporous silica (sol-gel, Vycor) [24] and in binary sodium silicate glasses $x\text{Na}_2\text{O}-(100-x)\text{SiO}_2$ with $x = 5$ and 15. It revealed the effect of nano-periodical chemical differentiation inside NGs in the $x = 15$ glass composition, with the Na concentrated near the nanoplanes [25,26]. Very recently, Wang et al. [27] showed the formation of NGs in sodium germanate (SG) glass with a 5Na₂O-95GeO₂ molar composition. Unlike in sodium silicate glasses, an increasing Na₂O content to 10 mol% was reported to prevent NG formation in these compositions.

In Ref. [28], the authors also investigated the formation of NGs in SG glasses, but for Na₂O contents ranging from 3 to 22 mol.%. They revealed aspects of their inscription drastically different from those in fused silica, although their structure is shown to have much in common. This is another exemplar that the glass composition has a critical effect on the NG writing conditions. Moreover, a minimal number of pulses required to induce form birefringence grows exponentially with the Na₂O content. The formation of NGs in 22Na₂O·78GeO₂ glass is accompanied with precipitation of Na₂Ge₄O₉ crystals inside and around them. For completeness, it must be pointed out that a form of birefringent nanostructure, appearing at a low pulse energy regime, has been recently observed by

Sakakura et al. [29] (labeled Type “X”, as opposed to “Type II” for NGs). It is a homogeneous production of asymmetric nanopores, oblate in the direction parallel to the laser polarization. One possible explanation is the destabilization of the oxide [30] or nanocavitation [31,32] by multiphoton ionization on lattice irregularities. The effect of nanopores flattening is attributed to near field enhancement with linear polarization [33]. For larger pulse energies (i.e., larger intensities), the induced plasma is observed to reorganize in arrays as predicted for higher energies [34,35] and drag the nanopores into nanoplanes.

A second type on NGs is found in oxide crystals and semiconductors (TeO_2 [12], Al_2O_3 [13], and Si [22]), where mostly arrangements of cracks, perpendicular to laser polarization, reveal the nanogratings. A third kind of NG is found in quartz crystal by periodic amorphization likely due to local fluctuations of thermal effect induced by the electron plasma structure [36]. Finally, a fourth kind of NG appears to be a partially crystalline non-periodic structures. They were observed, for example, in $33\text{Li}_2\text{O}-33\text{Nb}_2\text{O}_5-34\text{SiO}_2$ glasses (LNS glass precipitating LiNbO_3 , [15]), in $(33\text{Li}_2\text{O}-33\text{Nb}_2\text{O}_5-34-x\text{SiO}_2)-xB_2\text{O}_3$ glasses (LNSB non-congruent glasses) [37], in $65\text{Al}_2\text{O}_3-35\text{Dy}_2\text{O}_3$ glass (congruent glass composition for $\text{Dy}_3\text{Al}_5\text{O}_{12}$) [14], and in $20\text{Na}_2\text{O}-80\text{GeO}_2$ glasses (congruent glass composition for $\text{Na}_2\text{Ge}_4\text{O}_9$ [28]). Obviously, the periodicity arises from an interplay between multiphoton ionization and the glass constituents.

In the case of $20\text{Na}_2\text{O}-80\text{GeO}_2$ glasses, the crystallization occurs mainly around the NGs and in the experimental conditions of the study. However, it is not the case for $65\text{Al}_2\text{O}_3-35\text{Dy}_2\text{O}_3$ glasses, for which crystallization is inside the NG region, but the experimental resolution cannot bring up information on its distribution. As for LNS, the only noncongruent glass studied, the NGs are produced through an allotropic phase separation (SiO_2 lamellas and LiNbO_3 in between) [15]. A thorough study of this irradiated glass in Ref. [38] demonstrated that the spatial periodicity of the phase separation is influenced by the induced plasma. Indeed, it is much larger than the spontaneous one, i.e., simply induced by a temperature elevation. However, for NGs composed of nanopores or cracks such as in silica, there is no periodic chemical migration. Moreover, in all models describing the mechanisms on NG formation, there is no feature that can explain a phase separation, because the material is always considered homogeneous; just some defects can play a role in the mechanism by seeding a hot spot of nanoplasma [33] and triggering a local thermal effect. The distribution difference between positive and negative charges is not taken into account and cannot explain the influence of light on the phase separation [39]. For that purpose, in this paper, we consider the charge distribution induced upon light irradiation, analyzing more deeply compared to our previous publication and showing semi-quantitatively that the quasi-free electron plasma arrangement may interact with the phase separation, opening a way to its engineering.

2. Background

2.1. NG Structure

For suitable laser parameters that are described in Ref. [40], the previously depicted micro-to-nano structuring for LNS glass can be observed using transverse electron microscopy (bright field). The results, taken from Ref. [38] and displayed in Figure 2a, highlight the observed nanoplanes (i.e., nanogratings) oriented perpendicular to the laser polarization. Additionally, the chemical analyses reported in Figure 2b show that, for a suitable laser energy, there is alternation of rather pure silica nanoplanes. Between them, there is an important concentration of LiNbO_3 for high pulse energies or a small one (nanocrystals) surrounded by the original glass otherwise. Moreover, it must be recalled here that there is a difference of nanostructure between the matter irradiated (large spatial period) and the matter surrounding this irradiated volume but nevertheless heated by thermal diffusion from the irradiated volume (small period of the phase separation). We pinpoint this transition from one to the other in Figure 2c. At this transition, the thickness of the white (crystalline) lamellae decreases as one moves out of the focus point (i.e., away from the light), and new lamellae start to appear between them (the periodicity decreases). The

phase separation period decreases roughly from 100 nm to 10 nm. As the NG structuring appears in a large number of compounds and in several types of NG, we infer that the periodicity is imposed by the electron plasma structuring, in relation with some physical properties of the matter (still unknown to this date). The crystallization does not disturb the nanogratings organization. A direct deduction from this is that chemical separation is achieved before the crystallization.

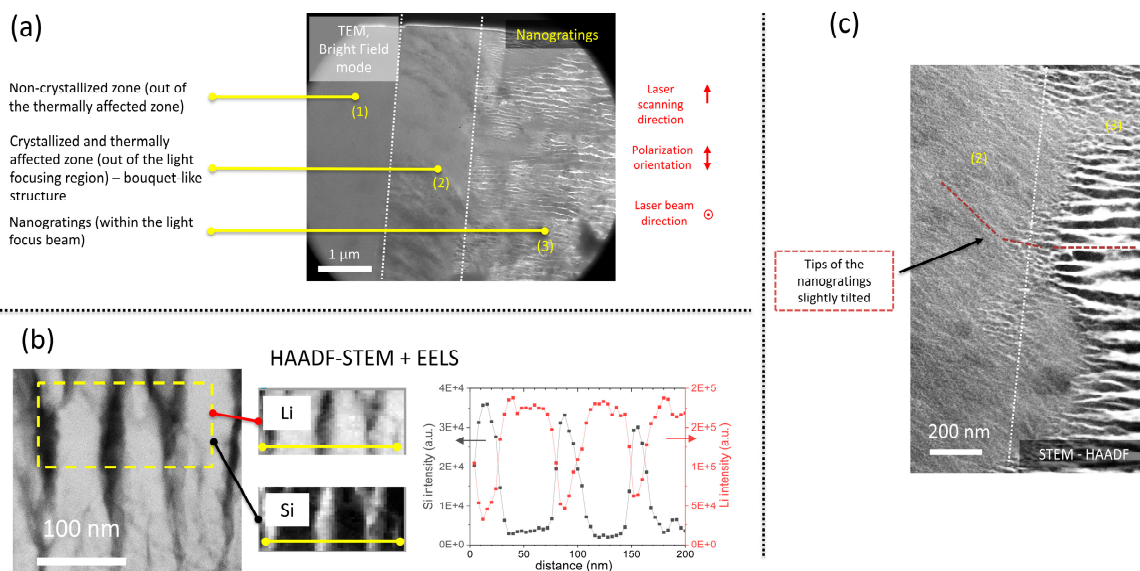


Figure 2. (a) Transverse electron microscope (TEM) micrograph in bright field mode of a part of the laser track in LNS glass. Irradiation conditions: 1030 nm, 1.8 μJ/pulse, 300 fs, 300 kHz, NA = 0.6, focusing depth = 350 μm, writing speed = 5 μm/s. Adapted from Ref. [38]. (b) Chemical distribution of Si and Li across lamellas using electron energy loss spectroscopy (EELS), (c) Topological relations between nanogratings and thermal crystallization out of the light-irradiated region (although close to it).

2.2. About the Plasma Spatial Structuring

Plasma structuring is carried out by photoionization of the solid during several pulses [41], with the help of levels in the bandgap created by the previous pulses [42]. This explains how the quasi-periodicity can be maintained along the laser scan [43], because the defects are gradually concentrated in certain areas, those where the electric charge density is the strongest. Moreover, all it takes is a few pulses and the plasma self-structures as calculated in silica glass in Ref. [43]. Nevertheless, the electron mobility must be sufficient to produce self-organization, and the ion mobility not excessively large to avoid annihilation of this structuring at high temperatures.

It is worth considering how the very short time period of a laser pulse may trigger an effect on the matter. In fact, at a scanning speed of a few μm/s and with a repetition rate of 100 kHz, the pulse density is on the order of 10^4 pulses/μm. Consequently, there is enough time to induce and maintain the fields, along with the induced potentials, which are imprinted in the solid. These fields will act in two ways: (i) thermodynamically by intervening on the constituent potentials and modifying the phase diagram and (ii) kinetically, by exerting forces on these constituents that can lead to structuring. A question that directly arises from this discussion is how does the plasma impose its structuring on the chemical separation?

3. Influence of the Electrostatic Field Induced by the Laser

In Ref. [43], the physical origin of the nanogratings in silica, constituted by nanopores arranged in quasi-periodic porous nanoplanes, is the cavitation of nanopores coupled to electromagnetic waves through temperature modulations perpendicular to the laser

polarization induced by electron plasma energy transfer to the lattice. There is no chemical diffusion in this scenario but a destabilization of SiO₂ at the place of high electron density where the energy deposition is thus the largest. Consequently, in this paper, we investigate an alternative route to the observed chemical separation, where the plasma imprints its spatial structure on the chemical separation achievement through electrochemical potential, leading to the uniformity of the Gibbs-free energy.

At the ultrashort time scale, the space modulation of the light-excited electrons is recognized as being trapped into the glass lattice and re-excited by the following pulse, thus reinforcing the nanograting structure.

If the plasma structure is achieved during a first pulse of a few 0.1 ps, 10 to 100 pulses are necessary for building a nanograting in pure silica lattice, as shown in Ref. [2], for example. This mechanism plays a memory role in the plasma structure formation and thus may develop transformations on a much longer time scale than during a single pulse duration. We suggest that the mechanism here starts similarly. However, we notice that, if the starting excitation follows the light intensity profile, this is no longer the case after several pulses. This means that positive ions produced at the beginning and negative ions produced by the electron trapping do not have the same distribution, yielding to an electric field modulation along the laser polarization direction.

The excited electrons have a large mobility and an excited lifetime large enough, whereas the positive counterparts are fixed to the lattice under the defect forms such as self-trapped holes or Oxygen Deficient Centers [42].

Based on the above discussion and to calculate the electric fields, we assume that the excited charges on a period of NG (Λ) are collected on a circular plate of infinitely small thickness. This is exemplified in Figure 3.

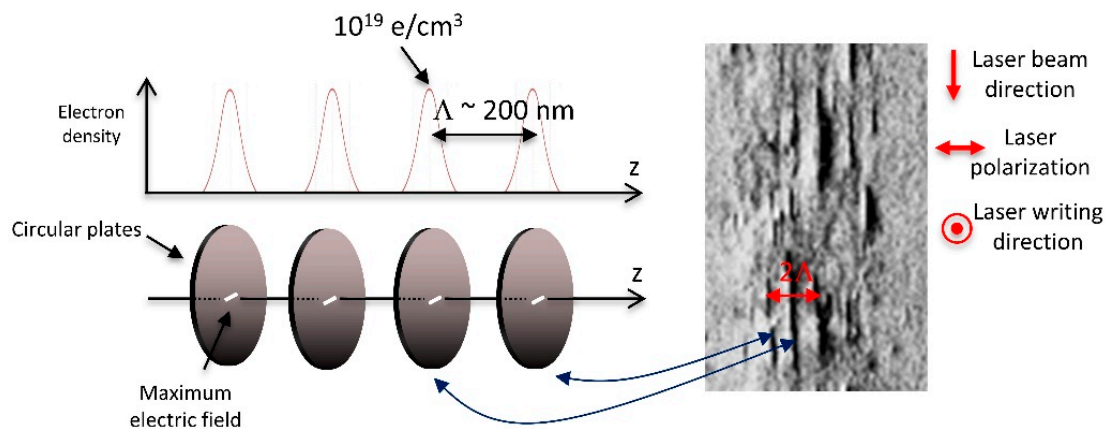


Figure 3. Scheme of the electron charge distribution along the nanogratings of period Λ . The relatively static cations exhibit a uniform charge density.

The electric field E_{Neg} , assumed to represent the electron accumulation into nano-disks can be calculated along the z axis, as represented in Figure 3. The electric field developed by a circular plate infinitely thin and the radius R (set as 1.5 μm , i.e., the beam radius) yields to the following classical expression:

$$E_{Neg}(z) = \frac{\sigma}{2\epsilon_0\epsilon_r} \left[\text{sign}(z) - \frac{z/R}{\sqrt{1 + (z/R)^2}} \right] \quad (1)$$

where σ is the surface charge density ($\sigma = -\Lambda\rho$, with Λ the spatial period of the NG around 200 nm and ρ the volume charge density of excited electrons), ϵ_0 , and ϵ_r (≈ 4 , see Appendix A) correspond to the vacuum and relative permittivity values, respectively.

The electric field of the positive counterpart, in turn, can be obtained assuming an homogeneous distribution on the period Λ . The expression is the following:

$$E_{Pos}(z) = \frac{\rho}{2\epsilon_0\epsilon_r} \int_{-\Lambda/2}^{\Lambda/2} \left[\text{sign}(z - za) - \frac{(z - za)/R}{\sqrt{1 + ((z - za)/R)^2}} \right] dza \quad (2)$$

By setting the variable $x = \frac{z-za}{R}$, the above expression can be integrated into the following form:

$$\text{that is read as } E_{Pos} = \frac{\rho R}{2\epsilon_0\epsilon_r} \left(f\left(\frac{z - \frac{\Lambda}{2}}{R}\right) - f\left(\frac{z + \frac{\Lambda}{2}}{R}\right) \right), \text{ with } f(x) = \sqrt{1 - x^2} - x \cdot \text{sign}(x). \quad (3)$$

The $\text{sign}(x)$ takes a value of -1 , 0 , or 1 when x is respectively negative, equal to zero, or positive.

Finally, to obtain the shape of the total electric field contributions, one simply needs to perform the sum of the two contributions (positive E_{Pos} + negative E_{Neg}). The results are displayed in Figure 4a, with individual contributions of E_{Pos} and E_{Neg} , and the sum of the two contributions. Moreover, a close up of the total electric field is provided in Figure 4b. As can be seen, especially from Figure 4b, the total electric field is confined in the period (from -100 to 100 nm). The amplitude (assuming $10^{19}/\text{cm}^3$ electron excited [44–46]) reaches ± 4500 V/ μm , which is a considerable field (around 1% of the characteristic atomic electric field strength $5.1 \cdot 10^5$ V/ μm [47]) that is probably partially rapidly screened by charged defects movement, even if the viscosity is sluggish. However, the plasma structure is recovered by the next pulse. On the other hand, the potential (assuming it is null at the infinity) reaches -200 V on the negative plate. Therefore, for a NG, the variation of the electric field and the potential along the axis of the NG appear as in Figure 4c. It is worth pointing out that the thickness of the negatively charged plate can be considered, instead of having an infinitely thin plate. This can be done by taking the expression of E_{Neg} similar to the one provided by E_{Pos} but by substituting $\Lambda = 200$ nm by 20 nm (i.e., typical for a lamella) and by multiplying the constant term in front of the integral by $-(\Lambda/e)$. This yields to a decrease of only $\sim 10\%$ of both the electric field and the potential values. Additionally, if the size of the lamellae is increased (i.e., R in Equation (1)), the value of the maximum and the shape of the total field does not change.

From the above results, such a large electric field has to be taken into account in the physicochemical reaction of phase separation processes. Here, there are two aspects of interest in the present observations. The first is the involvement of the electric field (E) in the phase separation (thermodynamic aspect). The second aspect is the migration of species in an electric field (kinetics aspect).

3.1. Thermodynamical Aspects

We have to analyze how E acts on the phase separation. We can show that phase separation is guided by the gain in generalized free energy (quoted \tilde{G}) that is the sum:

$$\tilde{G}(E) = \sum_i n_i \tilde{\mu}_i(E) \quad (4)$$

where n_i are the number of particles i , and $\tilde{\mu}_i$ corresponds to the generalized electrochemical potential expression (see Ref. [48] or [49]). By considering the problem as an electrostatic one, we can consider the following expression (please refer to the Appendix A for additional details):

$$\tilde{\mu}_i = \mu_i + z_i \mathcal{F} \phi + \frac{1}{2} \epsilon_0 E^2 \frac{\partial [(\epsilon_{r,g} - 1)V]}{\partial n_i}. \quad (5)$$

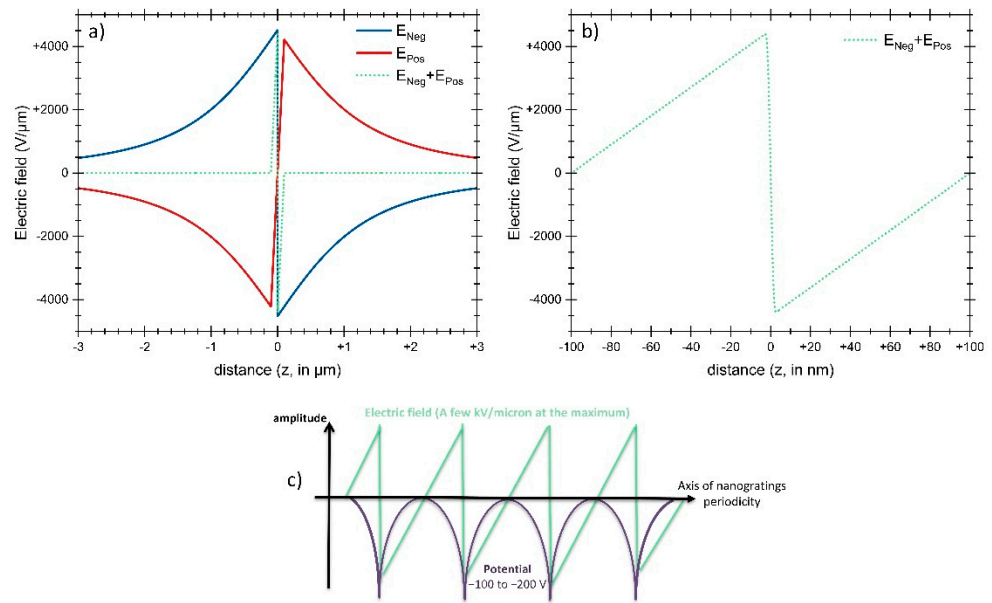


Figure 4. (a) Amplitude of the electric field for the negative and positive charges, along with the sum of the contributions as a function of the distance z (as in Figure 3), calculated from Equations (1) and (3), and their linear sum. The volume density of the excited electrons was set to $10^{19}/\text{cm}^3$ [44–46] and $R = 1.5 \mu\text{m}$. (b) Amplitude of the total electric field for one period, and (c) scheme of the electric field (E) and the electric potential (ϕ) distributions ($E = -\nabla\phi$).

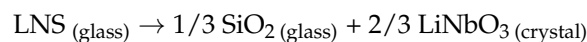
In the above expression, μ_i is the chemical potential, z_i is the charge of the species i , F the faraday constant, ϕ the electric potential, $\varepsilon_{r,g}$ the total relative permittivity of the glass, E the electric field with $E = -\nabla\phi$, and V the total volume of the system. It is demonstrated in the Appendix A that this expression can be rewritten under the following form:

$$\tilde{\mu}_i = \mu_i + z_i \mathcal{F} \phi + \frac{1}{2} \varepsilon_0 E^2 (\varepsilon_{r,i} - 1) \Omega_i, \quad (6)$$

where $\varepsilon_{r,g} = \sum_i \varepsilon_{r,i} \varphi_i$ with $\varepsilon_{r,i}$ is an effective permittivity, Ω_i is the partial molar volume of the i constituent, and φ_i is the volume fraction.

Here, we will consider that the glass is mainly covalent and composed of SiO_2 and LiNbO_3 group species and compare the electrostatic term of the energy variation with the chemical energy freed in the phase separation, which is of the order of a few kJ/mol [50] starting from the supercooled liquid or from the frozen glass.

Considering the example of this work, i.e., the formation of nanogratings in LNS glass, we must therefore consider the change of the energy balance, $\Delta\tilde{G}(E)$, in the following reaction:



The variation of the molar free energy gain in the process of crystallization, from the view of a solid-state transformation, is:

$$\Delta(\Delta\tilde{G}(E)) = \frac{1}{2} \varepsilon_0 E^2 \left[\frac{1}{3} \left((\varepsilon_{r,pure \text{SiO}_2} - 1) \Omega_{\text{pure SiO}_2} - (\varepsilon_{r,\text{SiO}_2 \text{ in glass}} - 1) \Omega_{\text{SiO}_2 \text{ in glass}} \right) + \frac{2}{3} \left((\varepsilon_{r,pure \text{LiNbO}_3} - 1) \Omega_{\text{pure LiNbO}_3} - (\varepsilon_{r,\text{LiNbO}_3 \text{ in glass}} - 1) \Omega_{\text{LiNbO}_3 \text{ in glass}} \right) \right]. \quad (7)$$

In this work, $\varepsilon_{r,pure \text{SiO}_2} = 2.12$ at 633 nm [51], and $\varepsilon_{r,pure \text{LiNbO}_3} = 5.31$ [52], which corresponds to an averaged value knowing that LiNbO_3 is a uniaxial crystal.

For the first member of the physicochemical reaction, relative to the glass, the permittivities are calculated in the Appendix A, considering as a starting point the linear additivity of the refractive index with respect to the volume fraction of the glass constituents [53]. We

calculated $\varepsilon_{r, \text{SiO}_2 \text{ in glass}} = 1,91$ and $\varepsilon_{r, \text{LiNbO}_3 \text{ in glass}} = 4.50$ and found that both values are lowered with respect to the ones in the pure solids. Consequently, the term $\Delta(\Delta\tilde{G}(E))$, from above, is positive. We point out that the refractive index values were taken at 633 nm in order to calculate $\varepsilon_{r, \text{LiNbO}_3 \text{ in glass}}$ from preexisting data. However, the results and the conclusions are not expected to change when considering the situation at 1030 nm, i.e., at the laser wavelength.

Considering the phase separation reaction and the aforementioned positive term, a high field stabilizes the glass with respect to the zero-field scenario. Consequently, the phase separation should be more effective in the low-field regions.

Noting that the coefficient $\frac{1}{2}\varepsilon_0 E^2$ may reach $\sim 9.10^{-2} \text{ kJ/cm}^3$ for the electric field previously calculated (4500 V/ μm), and considering our value of electric field and knowing the partial molar volumes (see Appendix A) $\Omega_{\text{pure SiO}_2} = 27.3 \text{ cm}^3/\text{mol}$, $\Omega_{\text{SiO}_2 \text{ in glass}} = 25.5 \text{ cm}^3/\text{mol}$, $\Omega_{\text{pure LiNbO}_3} = 31.7 \text{ cm}^3/\text{mol}$, $\Omega_{\text{LiNbO}_3 \text{ in glass}} = 34.4 \text{ cm}^3/\text{mol}$, we obtain $\Delta(\Delta\tilde{G}(E)) = 1.2 \text{ kJ/mol}$. This variation of the Gibbs free energy change for the reaction is on the order of magnitude of the energy released for the phase transformation to occur.

3.2. Kinetics Aspects

A correlated question is which one from SiO_2 or LiNbO_3 initially migrates, as a chemical migration is observed in the process of phase separation?

On that point, we have to consider the principle that elemental migrations are conducted under forces introduced by the electrochemical potential gradient. This is well known in the thermodynamics of irreversible phenomena, i.e., flux parts ($L_{ij}\vec{\nabla}\tilde{\mu}_j$ in the expression of \vec{J}_i) related to each force evolves such that fluxes either balance or vanish:

$$\vec{J}_i = \sum_j L_{ij}\vec{\nabla}\tilde{\mu}_j, \quad (8)$$

where L_{ij} are the Onsager coefficients.

Forces are proportionnal to $\vec{\nabla}\tilde{\mu}_j$; therefore, they are proportionnal to $\vec{E}\vec{\nabla}E$, as we do not consider charged species (LiNbO_3 and SiO_2). In the case of ionic migration, the term arising from the potential gradient is usually compensated by Fick diffusion. In this case, a uniform electric field may give rise to inhomogeneities, although starting from a homogeneous material. It is worth noting that forces induced by dipole polarization in this case would be null. However, in our situation, the electric field strongly varies in space, and the force is large enough to drive the dipole species towards the zero field region, provided their mobilities are large enough. The largest effect will be for the species with the largest relative molar permittivity (i.e., LiNbO_3).

In addition, if we compare the two situations, one for which SiO_2 is in the high-field region and LiNbO_3 in the low-field region, with the opposite case, the former constituent distribution is about 7 kJ/mol lower than for the latter one.

Following this line of reasoning, LiNbO_3 would thus concentrate between the charged lamellae over silica that would preferentially remain at the high-field regions. The equilibrium of the fluxes is established by chemical potential gradient resulting from the induced chemical inhomogeneities (Fick's law based on $\vec{\nabla}\mu$). When the low-field regions are sufficiently enriched enough in LiNbO_3 species, crystallization may occur. This explanation agrees with the experimental observations, as described in the above sections. A scheme of the proposed scenario is therefore shown in Figure 5.

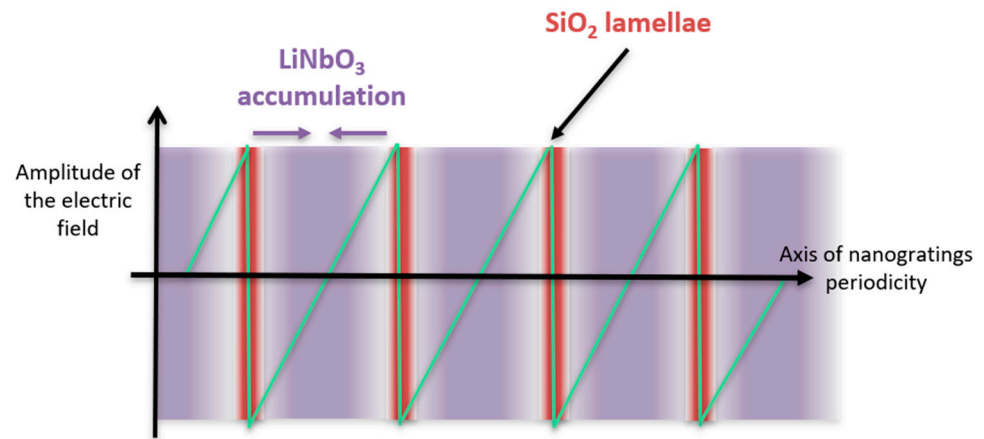


Figure 5. Representation of elemental migration of LiNbO_3 and SiO_2 with respect to the electric field amplitude along z axis (as in Figure 3).

Finally, we suggest that this process drives the LiNbO_3 migration that is extracted from the place of high electron density, that is, where the electric field is at its maximum. Reversely, under the effect of LiNbO_3 concentration gradient, SiO_2 migrates to high field region and pure silica lamellae are developed as it is observed in Figure 6a. This behavior agrees with the chemical reorganization observed in LNS [38]. The chemical composition of the remaining glass between lamellae is therefore impoverished in silica and, after a while, is ready for crystallization (Figure 6b). As shown in Ref. [38], the observed chemical separation in the irradiated region being influenced by the plasma spatial structuration is produced before any crystallization.

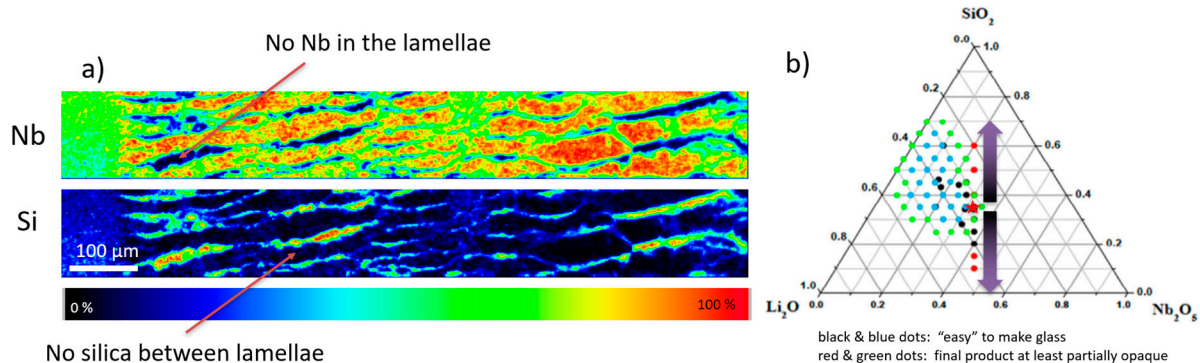


Figure 6. (a) chemical separation observed in the region of NG of Figure 2, and (b) phase separation during irradiation in the system $\text{Li}_2\text{O-Nb}_2\text{O}_5\text{-SiO}_2$. (black and red dots are from [54]. Green and blue dots data are redrawn from [55].

Then, crystallization texturing is induced by the peripheral solid—solid crystallization transformation for the laser parameters domain investigated here and as recalled earlier in this paper.

In such a model, an additional force (physical, not chemical), an electrostatic one, is developed from the self-organization of excited electron plasma. This force is superimposed with the thermal force (thermodynamical phase separation) and leads to a quasi-period of the chemical separation appearing larger than those observed under simple thermal treatment.

Therefore, we scheme below the revised mechanism, and the associated timescales, integrating several aspects from previous authors:

1. When the first pulse is deposited inside the material, over the several few fs, electrons are excited from the valence band to the conduction band through multiphoton ionization. Electron density in the conduction band increases until it saturates [56]. After

this “equilibrium” is reached, the remaining pulse energy deposited will compensate the energy loss due to electron relaxation. At this time, the fixed positive charges remain in the valence band, since they are bound to the lattice, while negative charges are located in the conduction band. Their lifetime, in the conduction band, is typically in the 100–200 fs range at low electron density [56] and of the order of ps for a high one [57].

2. On the other hand, the electron mobility can be considered of the order of $30 \text{ cm}^2/(\text{V}\cdot\text{s})$ [58]. This makes a maximum speed of a few 10^7 m/s with an electric field of the order of $\text{kV}/\mu\text{m}$, i.e., an electron can move over $\sim 100 \text{ nm}$ during $\sim 100 \text{ fs}$. A direct consequence is that electron plasma may reorganize or can be sensitive to the electromagnetic field during the rest of a sub-ps pulse, i.e., reorganized starting from a uniform electron density. According to the results and proposals from [33,35], electro-magnetic field concentration may appear in some random locations of the focal volume, including at point defects sites where the photoionization energy is weaker. Hot spots are formed under spherical nanoplasma [33].
3. Following this line of reasoning, the spherical nanoplasma is becoming oblate due to field enhancement effect described in [59], with the work of [60].
4. Then, long range interactions of the oblate nanoplasma are put into quasi-periodic gratings due to the fact that the interaction between nanoplasma are minimized perpendicularly to the light polarization (alignment into the nanoplane), whereas they are repulsed from each other along their short axis, i.e., along the laser polarization. At this stage, the plasma is roughly structured/organized, but this also corresponds to the end of the pulse duration. There are, therefore, now different distributions between positive and negative charges. As described above, the electrostatic force between them is compensated by negative–negative repulsion of nanoplasma, maintained by light concentration on the nanoplasma.
5. When the pulse deposition is over, the plasma structuring should disappear if the excited electron lifetimes were long enough for developing the organization. As mentioned above, it is in the ps (or less) timescale, so on the order of a pulse duration. This means that during plasma reorganization, there was an equilibrium between excitation and trapping, which inscribes the plasma structure progressively, but temporarily. When light goes away, all electrons relax and are permanently trapped on some structural changes in the lattice (produced by the hot spot, local heating). Note that for a typical 100 kHz repetition rate, the second pulse would be deposited $10 \mu\text{s}$ later, which is a much longer timescale compared to the timescales presently discussed. After the pulse, both negative and positive charge distributions are “recorded”, i.e., trapped in the lattice which exhibits a low mobility. The thermal stability now depends on the lattice temperature and the associated viscosity.
6. If the temperature decreases enough between pulses, such that the charge distribution is not destroyed, the negative charge carriers (fixed on structural defects) may act as sources to further seed a plasma during the subsequent pulses. From this view, the plasma structuring progresses towards a steady-state regime. This is the so called “memory effect”, introduced by [33]. From the aforementioned discussion, the lattice temperature–time dependence during the irradiation process must be discussed.
7. For this purpose, we can say first that the lattice temperature increases just after the pulse vanished, within a few ps. We consider a very simple model, such as a spherical heat source deposited in volume (few μm^3), and corresponding to the laser heat deposition in the focal volume. The physicochemical parameters of the LNS glass are taken from [61] (page 86, and recalled below), and the temperature is defined by the formula without heat accumulation i.e., the energy deposited vanishes during the period of time between two pulses. This is valid for period of a few μs . The expression is:

$$T(r, z, t) = T_A + T_{00} \cdot \frac{w^3}{(w^2 + 4D_{th} \cdot t)^{3/2}} \cdot \exp \left[- \left(\frac{r^2}{w^2 + 4D_{th} \cdot t} \right) \right], \quad (9)$$

$$\text{With } T_{00} = \frac{A \cdot E_p}{\pi^{\frac{3}{2}} \cdot \rho \cdot C_p w^3} \quad (10)$$

The parameters, along with their definition, are provided in Table 1.

Table 1. Parameters and typical values employed in LNS glass.

Parameters	Definitions	Value	Units
A	Fraction of the absorbed light	0.3	none
τ_D	Heat diffusion time $\tau_D = \frac{w^2}{4D_{th}}$ (decrease by 1/e)	0.53	μs
w	Beam waist radius (at 1/e)	1.5	μm
D_{Th}	Thermal diffusivity $D_{th} = \frac{\kappa}{\rho \cdot C_p}$	$1.06 \cdot 10^{-6}$	m^2/s
κ	Thermal conductivity	2.65	$\text{W}/(\text{m} \cdot \text{K})$
E_p	Pulse energy	0.5	μJ
ρ	Density	3830	kg/m^3
C_p	Specific heat capacity	650	$\text{J}/(\text{kg} \cdot \text{K})$
T_A	Ambiente temperature	20	$^{\circ}\text{C}$
T_m	Melting point	1260	$^{\circ}\text{C}$
T_g	Glass transition temperature	580, Ref. [62]	$^{\circ}\text{C}$

The reached maximal temperature $T_A + T_{00}$ (Equation (10)) remained during a fraction of diffusion time which is given in the table. It then decreases by 63% within 0.5 μs . We can understand that the maximum temperature does not overcome the boiling temperature as we have not detected any nanobubbles by TEM in our experiments.

Therefore, due to the temperatures reached, the glass viscosity will be small enough during the diffusion time to enable phase separation under the action of the electric field. One can estimate the migration length of the species for a time comparable to the diffusion time, using the well-known Stokes-Einstein equation $D_v = k_B T / (3\pi \cdot d \cdot \eta)$. In this expression, k_B is the Boltzmann's constant, T the temperature, D_v the diffusion coefficient, d the radius of the molecular species (calculated assuming a spherical volume and from a molar volume of $30 \text{ cm}^3/\text{mol}$), and η the viscosity. Following this, a characteristic length for the mobility of the species can be determined from the classical diffusion length $l_c = 2\sqrt{D_v \cdot t}$ with $t = \tau_p$. From this analysis, the diffusion length reached hundreds of nm. Furthermore, the presence of the electric field might increase this value.

Finally, the charge distribution decreases over the period, so is the electric field. In fact, it decreases at the same speed than $\text{SiO}_2\text{-LiNbO}_3$ phase separation is achieved. However, as opposed to the phase separation that progresses from one pulse to the other, the charge distribution is reinitiated by the subsequent pulse and thus drives the constituent separation. This separation is reinforced over a time corresponding to a few tens of pulses (order of magnitude), whereas the plasma structure evolves (in particular the spatial period of the nanogratings) in the same duration.

4. Conclusions

Among the different models proposed to describe the formation of nanogratings induced by femtosecond laser irradiation in glass, none of them consider the effect of charge redistribution due to high electronic mobility while the positive counterpart remains much lower (charged defects in the lattice). This paper takes into account the non-uniformity of excited electron density into the non-uniformity of electrochemical potential itself. From this view, we propose an explanation of how the formation of nanogratings are driven,

especially in LNS glass family that crystallizes non congruently. This work also proposes an interpretation on how the phase separation distance is larger in the laser-irradiated areas relative to a purely thermally driven crystallization process. These new insights on the nature of the chemical phase separation could be applied to other phase transitions, for a better control of nanogratings formation especially in systems for which crystallization properties are key aspects. Following the idea that excited electron charge density fluctuation drives the phase separation, we can predict that the organization of NG of chemical type may be perturbed by an external electric field. Furthermore, the existence of large electric field produced by mobility difference of oppositely charged carriers by light excitation open to consider that other effects may be at play such as electrostriction or inverse piezoelectricity. This may trigger deformation fields and contribute to cavitation and other stress fields that should be detected in some materials.

Author Contributions: Conceptualization, B.P.; methodology, B.P.; validation, M.C., B.P. and M.L.; formal analysis, B.P.; writing—original draft preparation, review and editing, M.C., B.P. and M.L. All authors have read and agreed to the published version of the manuscript.

Funding: This work was supported by the French National Research Agency under the program CHARMMAT ANR-11-LABX-0039-grant. Electron microscopy was carried out within the MAT-MECA project supported by the ANR under contract number ANR-10-EQPX-37.

Institutional Review Board Statement: Not applicable.

Informed Consent Statement: Not applicable.

Data Availability Statement: Data available upon reasonable request from the authors.

Conflicts of Interest: The authors declare no conflict of interest.

Appendix A

Expression of the electrochemical potential:

$$\tilde{G}(E) = \sum_i n_i \tilde{\mu}_i(E) \text{ with } \tilde{\mu}_i = \left(\frac{\partial \tilde{G}}{\partial n_i} \right)_{j \neq i} \text{ and,}$$

$\tilde{G}(E) = \sum_i n_i \mu_i + \sum_i n_i z_i \mathcal{F} \phi + \frac{1}{2} E \cdot P(E) \cdot V$ with $P(E) = \epsilon_0 (\epsilon_r - 1) E$, \mathcal{F} the Faraday, ϕ the electric potential, V the volume of the system. Therefore,

$$\tilde{\mu}_i = \mu_i + z_i \mathcal{F} \phi + \frac{1}{2} \epsilon_0 E^2 \frac{\partial [(\epsilon_r - 1) V]}{\partial n_i}$$

On the other hand, $V = \sum_i n_i \Omega_i$ with Ω_i the partial molar volume of the constituent i that we approximate to M_i / ρ_i with M_i the molar mass and ρ_i the specific mass. The total permittivity is not extensive and depends on the volume occupied by each constituent ($n_i \Omega_i$) with effective permittivities $\epsilon_{r,i}$. With such a definition, we get the following relation:

$\epsilon_{r,g} V = \sum_i \epsilon_{r,i} n_i \Omega_i$ so $\epsilon_{r,g} = \sum_i \epsilon_{r,i} \varphi_i$ with φ_i the volume fraction of the constituent i . $\varphi_i = \frac{n_i \Omega_i}{V} = \frac{x_i \Omega_i}{\sum_j x_j \Omega_j}$. The total permittivity is thus dependent on non independent

molar fraction. We finally get $(\epsilon_{r,g} - 1) V = \sum_i (\epsilon_{r,i} - 1) n_i \Omega_i$ and $\frac{\partial [(\epsilon_{r,g} - 1) V]}{\partial n_i} = (\epsilon_{r,i} - 1) \Omega_i$ assuming that effective permittivities depend only weakly on the chemical composition of the mixture. So, electrochemical potential expression becomes:

$$\tilde{\mu}_i = \mu_i + z_i \mathcal{F} \phi + \frac{1}{2} \epsilon_0 E^2 (\epsilon_{r,i} - 1) \Omega_i$$

Effective permittivity of the glass constituents in the glass phase.

We start using the basic assumption that the refractive index of a glass system is a linear function of the volume fractions of the constituents constituting such glass [53]. We

can write for the glass index the following relation assuming only constituent SiO₂ and LiNbO₃ of the glass with respective molar fraction 1/3 and 2/3:

$n_g = \varphi \cdot n_{SiO_2} + (1 - \varphi)n_{LiNbO_3}$ with φ the volume fraction of compound SiO₂ and n_{SiO_2} and n_{LiNbO_3} , the refractive index for each of the compounds. φ is given by $\varphi = \frac{\Omega_{SiO_2}x}{\Omega_{SiO_2}x + \Omega_{LiNbO_3, glass}(1-x)}$ with x , the molar fraction, and the partial molar volume $\Omega_i = \frac{M_i}{\rho_i}$. The partial molar volumes of the glass constituents LiNbO₃ and SiO₂ are calculated for the LNS glass stoichiometry ($x = 1/3$) using a polynomial fit of density measurements in [63] from 20%SiO₂ to 100%SiO₂ and taking the local ($x = 1/3$) slope end values (for LiNbO₃ and SiO₂). This gives a $\rho_{LiNbO_3, glass} = 4.25$ g/cm³ and $\Omega_{SiO_2, glass} = 25.5$ cm³/mol and $\Omega_{LiNbO_3, glass} = 34.4$ cm³/mol. (with $\rho_{SiO_2} = 2.2$ g/cm³, $M_{SiO_2} = 60.1$ g/mol, $M_{LiNbO_3} = 147.8$ g/mol). For the calculation of $\Omega_{pure SiO_2}$ and $\Omega_{pure LiNbO_3}$, the density values taken were respectively 2.20 g/cm³ and 4.64 g/cm³ [52].

The relative permittivity is given by $\varepsilon = n^2$. So, $\varepsilon_{r,g} = n_g^2$ and is thus a function of x only. While the value of n_g (SiO₂) is known one need to find the end value for a theoretical LiNbO₃ in glass. Following this, n_{LiNbO_3} in glass was deduced using the above equations (at 633 nm) from known values of $n_{SiO_2} = 1.457$ [51] and $n_g = 1.937$ [64]. This gives $n_{LiNbO_3, glass} = 2.131$.

Following the above, computation of the effective permittivity $\varepsilon_{r,i}$ can be done from the relation $\varepsilon_{r,g} = \sum_i \varepsilon_{r,i} \varphi_i$ knowing the total permittivity $\varepsilon_{r,g}$ for any value of x , by locally adjusting the expression $\varepsilon_{r,g} = \varphi \cdot \varepsilon_{r,SiO_2} + (1 - \varphi)\varepsilon_{r,LiNbO_3}$ around the proportion we are studying (1/3SiO₂, 2/3LiNbO₃) that we call x_0 assuming that $\varepsilon_{r,i}$ are not varying rapidly with x . We get the following expressions:

$$\varepsilon_{r,SiO_2} = \varepsilon_{r,g}(x_0) + \frac{\left(\frac{d\varepsilon_{r,g}}{dx}\right)_{x_0}}{\varphi} x(1-x)$$

$$\varepsilon_{r,LiNbO_3} = \varepsilon_{r,g}(x_0) - \frac{\left(\frac{d\varepsilon_{r,g}}{dx}\right)_{x_0}}{1-\varphi} x(1-x)$$

Finally, we get.

$$\varepsilon_{r,SiO_2} = 1,91 \text{ and } \varepsilon_{r,LiNbO_3} = 4.50$$

References

1. Shimotsuma, Y.; Kazansky, P.G.; Qiu, J.; Hirao, K. Self-Organized Nanogratings in Glass Irradiated by Ultrashort Light Pulses. *Phys. Rev. Lett.* **2003**, *91*, 247405. [CrossRef] [PubMed]
2. Desmarchelier, R.; Poumellec, B.; Brisset, F.; Mazerat, S.; Lancry, M. In the Heart of Femtosecond Laser Induced Nanogratings: From Porous Nanoplanes to Form Birefringence. *World J. Nano Sci. Eng.* **2015**, *5*, 115–125. [CrossRef]
3. Lancry, M.; Brisset, F.; Poumellec, B. In the heart of nanogratings made up during femtosecond laser irradiation. In *Bragg Gratings, Photosensitivity, and Poling in Glass Waveguides*; Optica Publishing Group: Washington, DC, USA, 2010; p. BWC3. [CrossRef]
4. Lancry, M.; Poumellec, B.; Chahid-Erjai, A.; Beresna, M.; Kazansky, P.G. Dependence of the femtosecond laser refractive index change thresholds on the chemical composition of doped-silica glasses. *Opt. Mater. Express* **2011**, *1*, 711–723. [CrossRef]
5. Shimotsuma, Y.; Asai, T.; Sakakura, M.; Miura, K. Femtosecond-Laser Nanostructuring in Glass. *J. Laser Micro/Nanoeng.* **2014**, *9*, 31–36. [CrossRef]
6. Zhang, F.; Zhang, H.; Dong, G.; Qiu, J. Embedded nanogratings in germanium dioxide glass induced by femtosecond laser direct writing. *J. Opt. Soc. Am. B* **2014**, *31*, 860–864. [CrossRef]
7. Asai, T.; Shimotsuma, Y.; Kurita, T.; Murata, A.; Kubota, S.; Sakakura, M.; Miura, K.; Brisset, F.; Poumellec, B.; Lancry, M. Systematic Control of Structural Changes in GeO₂ Glass Induced by Femtosecond Laser Direct Writing. *J. Am. Ceram. Soc.* **2015**, *98*, 1471–1477. [CrossRef]
8. Lancry, M.; Canning, J.; Cook, K.; Heili, M.; Neuville, D.R.; Poumellec, B. Nanoscale femtosecond laser milling and control of nanoporosity in the normal and anomalous regimes of GeO₂-SiO₂ glasses. *Opt. Mater. Express* **2016**, *6*, 321–330. [CrossRef]
9. Zimmermann, F.; Lancry, M.; Plech, A.; Richter, S.; Babu, B.H.; Poumellec, B.; Tünnermann, A.; Nolte, S. Femtosecond laser written nanostructures in Ge-doped glasses. *Opt. Lett.* **2016**, *41*, 1161–1164. [CrossRef]
10. Lancry, M.; Zimmerman, F.; Desmarchelier, R.; Tian, J.; Brisset, F.; Nolte, S.; Poumellec, B. Nanogratings formation in multicomponent silicate glasses. *Appl. Phys. B Laser Opt.* **2016**, *122*, 66. [CrossRef]

11. Richter, S.; Miese, C.; Döring, S.; Zimmermann, F.; Withford, M.J.; Tünnermann, A.; Nolte, S. Laser induced nanogratings beyond fused silica—Periodic nanostructures in borosilicate glasses and ULE™. *Opt. Mater. Express* **2013**, *3*, 1161–1166. [[CrossRef](#)]
12. Shimotsuma, Y.; Hirao, K.; Qiu, J.; Kazansky, P.G. Nano-modification inside transparent materials by femtosecond laser single beam. *Mod. Phys. Lett. B* **2005**, *19*, 225–238. [[CrossRef](#)]
13. Zhai, Q.; Ma, H.; Lin, X.; Li, Y.; Yin, W.; Tang, X.; Zeng, X.; Dai, Y. Evolution of self-organized nanograting from the pre-induced nanocrack-assisted plasma–laser coupling in sapphire. *Appl. Phys. B Laser Opt.* **2021**, *127*, 74. [[CrossRef](#)]
14. Shimotsuma, Y.; Mori, S.; Nakanishii, Y.; Kim, E.; Sakakura, M.; Miura, K. Self-assembled glass/crystal periodic nanostructure in Al₂O₃-Dy₂O₃ binary glass. *Appl. Phys. A* **2018**, *124*, 82. [[CrossRef](#)]
15. Cao, J.; Mazerolles, L.; Lancry, M.; Brisset, F.; Poumellec, B. Modifications in lithium niobium silicate glass by femtosecond laser direct writing: Morphology, crystallization, and nanostructure. *J. Opt. Soc. Am. B* **2016**, *34*, 160. [[CrossRef](#)]
16. Shimizu, M.; Nakanishi, Y.; Shimotsuma, Y.; Miura, K.; Sakakura, M. Formation mechanism of self-assembled polarization-dependent periodic nanostructures in β-Ga₂O₃. In Proceedings of the SPIE LASE, San Francisco, CA, USA, 27 January–1 February 2018; Volume 10520, p. 105201. [[CrossRef](#)]
17. Ahn, M.; Sarracino, A.; Ansari, A.; Torralva, B.; Yalisove, S.; Phillips, J. Unique material modifications of Ga₂O₃ enabled by ultrafast laser irradiation. In Proceedings of the SPIE OPTO, San Francisco, CA, USA, 1–6 February 2020; Volume 11281, pp. 28–35.
18. Yao, H.; Zaiter, R.; Cavillon, M.; Delullier, P.; Lu, B.; Cardinal, T.; Dai, Y.; Poumellec, B.; Lancry, M. Formation of nanogratings driven by ultrafast laser irradiation in mid-IR heavy oxide glasses. *Ceram. Int.* **2022**, *48*, 31363–31369. [[CrossRef](#)]
19. Xie, Q.; Cavillon, M.; Pugliese, D.; Janner, D.; Poumellec, B.; Lancry, M. On the Formation of Nanogratings in Commercial Oxide Glasses by Femtosecond Laser Direct Writing. *Nanomaterials* **2022**, *12*, 2986. [[CrossRef](#)]
20. Wang, Y.; Wei, S.; Cicconi, M.R.; Tsuji, Y.; Shimizu, M.; Shimotsuma, Y.; Miura, K.; Peng, G.-D.; Neuville, D.R.; Poumellec, B.; et al. Femtosecond laser direct writing in SiO₂-Al₂O₃ binary glasses and thermal stability of Type II permanent modifications. *J. Am. Ceram. Soc.* **2020**, *103*, 4286–4294. [[CrossRef](#)]
21. Wang, Y.; Cavillon, M.; Ballato, J.; Hawkins, T.; Elsmann, T.; Rothhardt, M.; Desmarchelier, R.; Laffont, G.; Poumellec, B.; Lancry, M. 3D Laser Engineering of Molten Core Optical Fibers: Toward a New Generation of Harsh Environment Sensing Devices. *Adv. Opt. Mater.* **2022**, *10*, 2200379. [[CrossRef](#)]
22. Shimotsuma, Y.; Nakanishi, Y.; Skakura, M.; Miura, K. Self-assembled periodic nanostructures embedded in wide bandgap semiconductor. In Proceedings of the 2017 Conference on Lasers and Electro-Optics Pacific Rim (CLEO-PR), Singapore, 31 July–4 August 2017; pp. 1–3. [[CrossRef](#)]
23. Fedotov, S.; Lipatiev, A.; Lipateva, T.; Lotarev, S.; Mel'nikov, E.; Sigaev, V. Femtosecond laser-induced birefringent microdomains in sodium-borate glass for highly secure data storage. *J. Am. Ceram. Soc.* **2021**, *104*, 4297–4303. [[CrossRef](#)]
24. Cerkauskaite, A.; Drevinskas, R.; Rybaltovskii, A.O.; Kazansky, P.G. Ultrafast laser-induced birefringence in various porosity silica glasses: From fused silica to aerogel. *Opt. Express* **2017**, *25*, 8011. [[CrossRef](#)]
25. Lotarev, S.; Fedotov, S.; Lipatiev, A.; Presnyakov, M.; Kazansky, P.; Sigaev, V. Light-driven nanoprototypical modulation of alkaline cation distribution inside sodium silicate glass. *J. Non-Crystalline Solids* **2018**, *479*, 49–54. [[CrossRef](#)]
26. Fedotov, S.S.; Lipat'ev, A.S.; Lotarev, S.V.; Sigaev, V.N. Local Formation of Birefringent Structures in Alkali-Silicate Glass by Femtosecond Laser Beam. *Glas. Ceram.* **2017**, *74*, 227–229. [[CrossRef](#)]
27. Wang, J.; Liu, X.; Dai, Y.; Wang, Z.; Qiu, J. Effect of sodium oxide content on the formation of nanogratings in germanate glass by a femtosecond laser. *Opt. Express* **2018**, *26*, 12761–12768. [[CrossRef](#)]
28. Lotarev, S.V.; Fedotov, S.S.; Kurina, A.I.; Lipatiev, A.S.; Sigaev, V.N. Ultrafast laser-induced nanogratings in sodium germanate glasses. *Opt. Lett.* **2019**, *44*, 1564–1567. [[CrossRef](#)] [[PubMed](#)]
29. Sakakura, M.; Lei, Y.; Wang, L.; Yu, Y.-H.; Kazansky, P.G. Ultralow-loss geometric phase and polarization shaping by ultrafast laser writing in silica glass. *Light. Sci. Appl.* **2020**, *9*, 1–10. [[CrossRef](#)] [[PubMed](#)]
30. Lancry, M.; Poumellec, B.; Canning, J.; Cook, K.; Poulin, J.-C.; Brisset, F. Ultrafast nanoporous silica formation driven by femtosecond laser irradiation. *Laser Photon.-Rev.* **2013**, *7*, 953–962. [[CrossRef](#)]
31. Xie, Q.; Cavillon, M.; Poumellec, B.; Pugliese, D.; Janner, D.; Lancry, M. Application and validation of a viscosity approach to the existence of nanogratings in oxide glasses. *Opt. Mater.* **2022**, *130*, 112576. [[CrossRef](#)]
32. Rudenko, A.; Colombier, J.-P.; Itina, T.E. Nanopore-mediated ultrashort laser-induced formation and erasure of volume nanogratings in glass. *Phys. Chem. Chem. Phys.* **2018**, *20*, 5887–5899. [[CrossRef](#)]
33. Rajeev, P.; Gertsvolf, M.; Hnatovsky, C.; Simova, E.; Taylor, R.; Corkum, P.; Rayner, D.; Bhardwaj, V. Transient nanoplasmonics inside dielectrics. *J. Phys. B At. Mol. Opt. Phys.* **2007**, *40*, S273. [[CrossRef](#)]
34. Beresna, M.; Gecevicius, M.; Kazansky, P.G.; Taylor, T.; Kavokin, A.V. Exciton mediated self-organization in glass driven by ultrashort light pulses. *Appl. Phys. Lett.* **2012**, *101*, 053120. [[CrossRef](#)]
35. Cang, H.; Labno, A.; Lu, C.; Yin, X.; Liu, M.; Gladden, C.; Liu, Y.; Zhang, X. Probing the electromagnetic field of a 15-nanometre hotspot by single molecule imaging. *Nature* **2011**, *469*, 385–388. [[CrossRef](#)]
36. Zhang, F.; Nie, Z.; Huang, H.; Ma, L.; Tang, H.; Hao, M.; Qiu, J. Self-assembled three-dimensional periodic micro-nano structures in bulk quartz crystal induced by femtosecond laser pulses. *Opt. Express* **2019**, *27*, 6442–6450. [[CrossRef](#)] [[PubMed](#)]

37. Muzi, E.; Cavillon, M.; Lancry, M.; Brisset, F.; Sapaly, B.; Janner, D.; Poumellec, B. Polarization-oriented LiNbO₃ nanocrystals by femtosecond laser irradiation in LiO₂-Nb₂O₅-SiO₂-B₂O₃ glasses. *Opt. Mater. Express* **2021**, *11*, 1313–1320. [[CrossRef](#)]
38. Cavillon, M.; Cao, J.; Vallet, M.; Brisset, F.; Mazerolles, L.; Dkhil, B.; Lancry, M.; Poumellec, B. Thermal and Electron Plasma Effects on Phase Separation Dynamics Induced by Ultrashort Laser Pulses. *Crystals* **2022**, *12*, 496. [[CrossRef](#)]
39. Rudenko, A.; Ma, H.; Veiko, V.P.; Colombier, J.-P.; Itina, T.E. On the role of nanopore formation and evolution in multi-pulse laser nanostructuring of glasses. *Appl. Phys. A* **2017**, *124*, 63. [[CrossRef](#)]
40. Cao, J.; Lancry, M.; Brisset, F.; Mazerolles, L.; Saint-Martin, R.; Poumellec, B. Femtosecond Laser-Induced Crystallization in Glasses: Growth Dynamics for Orientable Nanostructure and Nanocrystallization. *Cryst. Growth Des.* **2019**, *19*, 2189–2205. [[CrossRef](#)]
41. Mao, S.; Quéré, F.; Guizard, S.; Mao, X.; Russo, R.; Petite, G.; Martin, P. Dynamics of femtosecond laser interactions with dielectrics. *Appl. Phys. A* **2004**, *79*, 1695–1709. [[CrossRef](#)]
42. Lancry, M.; Poumellec, B.; Desmarchelier, R.; Bourguignon, B. Oriented creation of anisotropic defects by IR femtosecond laser scanning in silica. *Opt. Mater. Express* **2012**, *2*, 1809–1821. [[CrossRef](#)]
43. Rudenko, A.; Colombier, J.; Itina, T.E.; Stoian, R. Genesis of Nanogratings in Silica Bulk via Multipulse Interplay of Ultrafast Photo-Excitation and Hydrodynamics. *Adv. Opt. Mater.* **2021**, *9*, 2100973. [[CrossRef](#)]
44. Fernandez, T.; Sakakura, M.; Eaton, S.; Sotillo, B.; Siegel, J.; Solis, J.; Shimotsuma, Y.; Miura, K. Bespoke photonic devices using ultrafast laser driven ion migration in glasses. *Prog. Mater. Sci.* **2017**, *94*, 68–113. [[CrossRef](#)]
45. Couairon, A.; Sudrie, L.; Franco, M.; Prade, B.; Mysyrowicz, A. Filamentation and damage in fused silica induced by tightly focused femtosecond laser pulses. *Phys. Rev. B* **2005**, *71*, 125435. [[CrossRef](#)]
46. Huang, F.; Si, J.; Chen, T.; Shen, T.; Shi, M.; Hou, X. Temporal-spatial dynamics of electronic plasma in femtosecond laser induced damage. *Opt. Express* **2021**, *29*, 14658–14667. [[CrossRef](#)] [[PubMed](#)]
47. Boyd, R.W. Chapter 1-The Nonlinear Optical Susceptibility. In *Nonlinear Optics*, 3rd ed.; Boyd, R.W., Ed.; Academic Press: Burlington, NJ, USA, 2008; pp. 1–67.
48. Uda, S.; Huang, X.; Koh, S. Transformation of the incongruent-melting state to the congruent-melting state via an external electric field for the growth of langasite. *J. Cryst. Growth* **2005**, *281*, 481–491. [[CrossRef](#)]
49. Han, G.; Wang, H. Generalized expression of chemical potential with influence of external fields and its applications: Effect of charged particles on droplet condensation. *Fluid Phase Equilibria* **2013**, *338*, 269–273. [[CrossRef](#)]
50. Hicher, P. The Growth of Oxide Crystals under Electric Field. Ph.D. Thesis, Université Paris Saclay (COMUE), Gif-sur-Yvette, France, 2016.
51. Malitson, I.H. Interspecimen comparison of the refractive index of fused silica. *J. Opt. Soc. Am.* **1965**, *55*, 1205–1209. [[CrossRef](#)]
52. Wong, K.K. *Properties of Lithium Niobate*; INSPEC: London, UK, 2002.
53. Dragic, P.D.; Cavillon, M.; Ballato, A.; Ballato, J. A unified materials approach to mitigating optical nonlinearities in optical fiber. II. A. Material additivity models and basic glass properties. *Int. J. Appl. Glas. Sci.* **2017**, *9*, 278–287. [[CrossRef](#)]
54. Fan, C. Contribution to Nano or Micro Crystallization Induction in Silica-Based Glass by Femtosecond Laser Irradiation. Ph.D. Thesis, Université Paris Sud-Paris XI, Bures-sur-Yvette, France, East China University of Science and Technology, Shanghai, China, 2012.
55. Maksimova, O.S.; Korzunova, L.V.; Milberg, Z.P. Properties and structure of glasses of the system Li₂O-Nb₂O₅-SiO₂. *Izv. Akad. Nauk Latv. SSR Ser. Khim* **1975**, *5*, 530–534.
56. Lancry, M.; Groothoff, N.; Poumellec, B.; Guizard, S.; Fedorov, N.; Canning, J. Time-resolved plasma measurements in Ge-doped silica exposed to infrared femtosecond laser. *Phys. Rev. B* **2011**, *84*, 245103. [[CrossRef](#)]
57. Mauclair, C.; Mermillod-Blondin, A.; Mishchik, K.; Bonse, J.; Rosenfeld, A.; Colombier, J.P.; Stoian, R. Excitation and relaxation dynamics in ultrafast laser irradiated optical glasses. *High Power Laser Sci. Eng.* **2016**, *4*, 46. [[CrossRef](#)]
58. Goodman, A.M. Electron Hall Effect in Silicon Dioxide. *Phys. Rev.* **1967**, *164*, 1145–1150. [[CrossRef](#)]
59. Bhardwaj, V.R.; Simova, E.; Rajeev, P.P.; Hnatovsky, C.; Taylor, R.S.; Rayner, D.M.; Corkum, P.B. Optically Produced Arrays of Planar Nanostructures inside Fused Silica. *Phys. Rev. Lett.* **2006**, *96*, 057404. [[CrossRef](#)] [[PubMed](#)]
60. Boyd, G.T.; Rasing, T.; Leite, J.R.R.; Shen, Y.R. Local-field enhancement on rough surfaces of metals, semimetals, and semiconductors with the use of optical second-harmonic generation. *Phys. Rev. B* **1984**, *30*, 519–526. [[CrossRef](#)]
61. Que, R. Demonstration of Anisotropy Control of Optical Properties Induced by IR fs Laser Irradiation in Organic Materials: Birefringence, Di-attenuation, SHG, Photoluminescence. Doctoral Dissertation, Université Paris-Saclay, Gif-sur-Yvette, France, 2022.
62. Muzi, E.; Cavillon, M.; Lancry, M.; Brisset, F.; Que, R.; Pugliese, D.; Janner, D.; Poumellec, B. Towards a Rationalization of Ultrafast Laser-Induced Crystallization in Lithium Niobium Borosilicate Glasses: The Key Role of the Scanning Speed. *Crystals* **2021**, *11*, 290. [[CrossRef](#)]

63. Prapitpongwanich, P.; Pengpat, K.; Rüssel, C. Phase separation and crystallization in LiNbO₃/SiO₂ glasses. *Mater. Chem. Phys.* **2009**, *113*, 913–918. [[CrossRef](#)]
64. Cao, J.; Brisset, F.; Mazerolles, L.; Lancry, M.; Poumellec, B. Creation and orientation of nano-crystals by femtosecond laser light for controlling optical non-linear response in silica-based glasses. In *Création et Orientation de Nano-Cristaux par Irradiation Laser Femtoseconde pour le Contrôle de L'orientation des Propriétés Op-tiques Non-Linéaires dans des Verres à Base de Silice*; Université Paris Saclay: Gif sur Yvette, France, 2017.

Disclaimer/Publisher's Note: The statements, opinions and data contained in all publications are solely those of the individual author(s) and contributor(s) and not of MDPI and/or the editor(s). MDPI and/or the editor(s) disclaim responsibility for any injury to people or property resulting from any ideas, methods, instructions or products referred to in the content.